International Journal of QUANTUM CHEMISTRY

Ab Initio Chemical Kinetics for the Unimolecular Decomposition of Si_2H_5 Radical and Related Reverse Bimolecular Reactions

Shang-Ying Wu,[a] Yun-Min Lee,[a] Jong-Shinn Wu,[a] and Ming-Chang Lin*[b,c]

For plasma enhanced and catalytic chemical vapor deposition (PECVD and Cat-CVD) processes using small silanes as precursors, disilanyl radical (Si_2H_5) is a potential reactive intermediate involved in various chemical reactions. For modeling and optimization of homogeneous a-Si:H film growth on large-area substrates, we have investigated the kinetics and mechanisms for the thermal decomposition of Si_2H_5 producing smaller silicon hydrides including SiH, SiH_2, SiH_3, and Si_2H_4, and the related reverse reactions involving these species by using *ab initio* molecular-orbital calculations. The results show that the lowest energy path is the production of $SiH + SiH_4$ that proceeds via a transition state with a barrier of 33.4 kcal/mol relative to Si_2H_5. Additionally, the dissociation energies for breaking the Si—Si and H—SiH_2 bonds were predicted to be 53.4 and 61.4 kcal/mol, respectively. To validate the predicted enthalpies of reaction, we have evaluated the enthalpies of formation for SiH, SiH_2, $HSiSiH_2$, and $Si_2H_4(C_{2h})$ at 0 K by using the isodesmic reactions, such as $^2HSiSiH_2 + {}^1C_2H_6 \rightarrow {}^1Si_2H_6 + {}^2HCCH_2$ and $^1Si_2H_4(C_{2h}) + {}^1C_2H_6 \rightarrow {}^1Si_2H_6 + {}^1C_2H_4$. The results of SiH (87.2 kcal/mol), SiH_2 (64.9 kcal/mol), $HSiSiH_2$ (98.0 kcal/mol), and Si_2H_4 (68.9 kcal/mol) agree reasonably well previous published data. Furthermore, the rate constants for the decomposition of Si_2H_5 and the related bimolecular reverse reactions have been predicted and tabulated for different T, P-conditions with variational Rice–Ramsperger–Kassel–Marcus (RRKM) theory by solving the master equation. The result indicates that the formation of $SiH + SiH_4$ product pair is most favored in the decomposition as well as in the bimolecular reactions of $SiH_2 + SiH_3$, $HSiSiH_2 + H_2$, and $Si_2H_4(C_{2h}) + H$ under T, P-conditions typically used in PECVD and Cat-CVD. © 2013 Wiley Periodicals, Inc.

DOI: 10.1002/qua.24557

Introduction

In the semiconductor industry, deposition of layers of silicon-based thin films is a widely adopted integral technology using either the plasma enhanced chemical vapor deposition (PECVD) or catalytic chemical vapor deposition (Cat-CVD) method.[1–3] Fundamental modeling of fluid dynamics and chemical reaction mechanisms is often required to understand the complex chemical processes occurring inside the CVD chamber for further optimization of the processes. The success of modeling requires detailed chemical kinetics with reliable rate constants for key reactions involved. Measurements of these rate constants may be possible, but it is often very expensive or difficult. The recent progress in *ab initio* calculations has made reliable predictions of rate constants possible and efficient. The objective of this article is to provide the kinetic data for the unimolecular decomposition of Si_2H_5 and its related reverse bimolecular reactions involving SiH, SiH_2, SiH_3, and Si_2H_3 radicals using *ab initio* calculations. These radicals are known to coexist in CVD media for a-Si:H thin film growth with small silanes as precursors.[1–3]

In a typical CVD process, the reactions may include the dissociation of source gases induced by electron collisions in a plasma environment, radicals reactions with silicon compounds, the thermal decomposition of compounds, and so on.[4–7] For silicon-based film deposition, silane (SiH_4) is often used as the gas source; the disilanyl (Si_2H_5) radical may be generated by H-atom abstraction by H or other radicals from the disilane (Si_2H_6) formed by the recombination of SiH_3 radicals or the association of SiH_3 with SiH_2 radical, among others.[8–10] The chemical properties of the transient silicon hydrides, Si_2H_5, Si_2H_4, Si_2H_3, and Si_2H_2 prepared from fluorine atom reactions with disilane were first investigated and measured with the photoionization mass spectrometry method by Ruscic and Berkowitz.[11] In addition, they summarized the previous Si_2H_n, ($n = 2$–5) structures with *ab initio* calculations and provided the enthalpies of formation derived by combining their ionization potentials with obtained appearance potentials and that of Si_2H_6 from previous works. Jasinski et al.[4] reviewed the various gas-phase reactions regarding monosilicon hydride radicals. A rate constant of $\sim 3 \times 10^{-12}$

[a] *S.-Y. Wu, Y.-M. Lee, J. S. Wu*
Department of Mechanical Engineering, National Chiao Tung University, Hsinchu 300, Taiwan
[b] *M. C. Lin*
Department of Applied Chemistry, Center for Interdisciplinary Molecular Science, National Chiao Tung University, Hsinchu 300, Taiwan
E-mail: chemmcl@emory.edu
[c] *M. C. Lin*
Department of Chemistry, Emory University, Atlanta, Georgia 30322, USA

cm^3 $molecule^{-1}$ s^{-1} at 500 K in the low pressure range for the reaction of silylidyne (SiH) with silane (SiH_4) was estimated. Recently, Sillars et al.[12] presented an experimental and theoretical study on the Si_2H_5 radical. The molecular structures, vibrational frequencies, and relative energy estimates of Si_2H_5, $H_2SiHSiH_2$ (transition state, TS), and $HSiHSiH_3$ (C_1) were also computed with electronic structure methods using the Gaussian 98 program. However, no related kinetic data were predicted.

In this study, we attempt to investigate the elementary reactions relevant to the thermal decomposition of the Si_2H_5 radical and its related reverse bimolecular processes. The dissociation of Si_2H_5 to elementary silicon hydride radicals are considered as follows:

$$Si_2H_5 \rightarrow SiH + SiH_4 \quad (1)$$

$$\rightarrow HSiSiH_2 + H_2 \quad (2)$$

$$\rightarrow SiH_3 + SiH_2 \quad (3)$$

$$\rightarrow Si_2H_4(C_{2h}) + H \quad (4)$$

and their reverse reactions are also considered, such as,

$$SiH + SiH_4 \rightarrow Si_2H_5* \rightarrow \text{products} \quad (5)$$

$$SiH_2 + SiH_3 \rightarrow Si_2H_5* \rightarrow \text{products} \quad (6)$$

$$HSiSiH_2 + H_2 \rightarrow Si_2H_5* \rightarrow \text{products} \quad (7)$$

$$Si_2H_4 + H \rightarrow Si_2H_5* \rightarrow \text{products} \quad (8)$$

In the above reactions, "Si_2H_5*" represents internally excited disilanyl radical formed by bimolecular radical association reactions Eqs. (5–8) and the "products" represent all possibly product pairs which can be formed in each reverse reaction via the Si_2H_5* intermediate as depicted in the potential energy surface (PES) to be discussed later. Additionally, the calculated enthalpies of reaction including isodesmic reactions will be used to deduce the enthalpies of formation for silicon hydride species involved; these results will be validated by comparison with the published data wherever possible. Finally, temperature and pressure-dependent rate constants over a wide range of conditions, including those which are generally applied to deposition by PECVD and Cat-CVD processes, will be predicted by statistical theory based on PES computed by high-level quantum chemical calculations discussed below.

Computational Methods

Ab initio MO calculations

The geometries of the reactants, products, and TSs for the disilanyl (Si_2H_5) thermal decomposition reaction were optimized by using density functional theory using Becke's three parameter nonlocal exchange functions with the nonlocal correlation functions of Lee, Yang and Parr method (B3LYP)[13–15] with the 6–311++G(3df,2p) basis set. This calculation was further improved by the coupled-cluster method using single, double, and perturbative triple excitations (CCSD(T))[16a] with the 6–311+G(d,p)[16b] basis set. Vibrational frequencies of all species were also computed at the same level of theory to characterize stationary points and zero-point energy (ZPE) corrections. The geometries of TSs were verified by their connectivity with the reactants and products using the intrinsic reaction coordinate calculations.[17,18] To obtain reliable energies, the single-point energy calculations of the stationary points were executed at the CCSD(T)/6–311++G(3df,2p) level of theory based on the optimized geometries using the CCSD/6–311++G(d,p) method. Complete basis set (CBS[19,20]) extrapolation technique was also used for further improving the energy accuracy. The basis set extrapolation was based on the calculations with the aug-cc-pVXZ (X = D, T, and Q) basis using the CCSD(T) optimized geometries. The CBS energies have been estimated using three-point extrapolation scheme, $E(X) = E_{CBS} + b\exp[-(X-1)] + c\exp[-(X-1)^2]$ where X is the cardinal number of the basis sets associated with $X = 2$ (DZ) (double Zeta), 3 (TZ) (triple Zeta), 4 (QZ) (quadruple Zeta), and E_{CBS} is the asymptotic value to approximate the CBS limit. The Gaussian 03 quantum chemical software was used throughout the study.[21]

Kinetics methods

For the barrierless reactions, the canonical variational TS theory (CVTST)[22–24] was used to minimize rate coefficients. The CVTST rate coefficient equation in the quasi-thermodynamic form could be expressed by

$$k(T,s) = \alpha(k_bT/h)\ \exp\ (-\Delta G^\circ(T,s)/k_bT) \quad (9)$$

where s is the distance along the minimum energy path (MEP), with the saddle point at $s = 0$, the reactants region corresponding to $s < 0$ and the products region corresponding to $s > 0$. α is statistical factor and k_b is the Boltzmann constant. T is the temperature, h is Planck's constant, and $\Delta G^\circ(T,s)$ is a quasi-thermodynamic quantity (Gibbs standard free energy of activation). The condition for minimizing $k(T,s)$ is equivalent to maximizing the free energy activation. The Gibbs standard free energy functions were determined using the thermodynamic functions of NIST-JANAF Thermochemical Tables.[25] Furthermore, the pressure-dependent rate constants were calculated with the RRKM theory[22–24,26,27] by solving the master equation with the VARIFLEX program suite.[28] The microcanonical rate coefficient of the standard RRKM form is expressed as a function of total energy E and angular momentum quantum number J by

$$k(E,J) = \frac{N^{\ddagger}(E,J)}{h\rho(E,J)} \quad (10)$$

where $N^{\ddagger}(E,J)$ is the TS's sum of states, $\rho(E,J)$ is the density of states of activated reactants, and again h is Planck's constant. Then, one-dimensional master equations were solved to determine the nonequilibrium distribution functions for each channel.

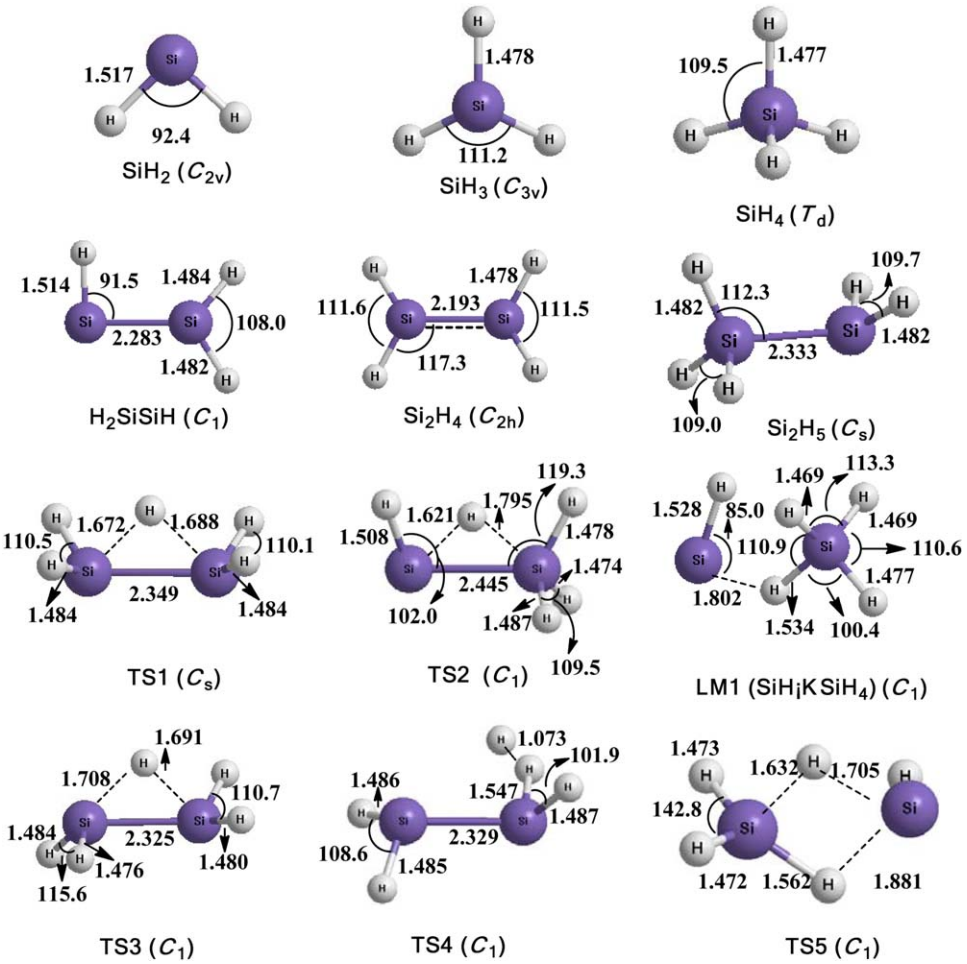

Figure 1. Optimized geometric parameters of various stationary points for Si_2H_5 thermal decomposition reaction calculated at the CCSD(T)/6–311+G(d,p) level. Bond lengths are in angstroms and angles are in degrees. [Color figure can be viewed in the online issue, which is available at wileyonlinelibrary.com.]

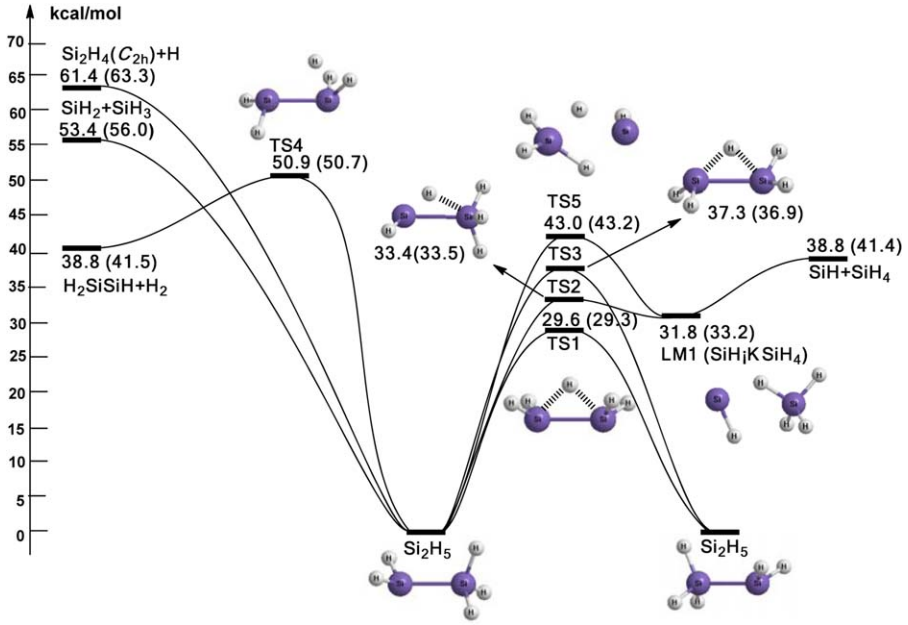

Figure 2. Potential energy diagram of the Si_2H_5 thermal decomposition reaction. Relative energies (kcal/mol) calculated at the CCSD(T)/6–311++G(3df,2p)//CCSD(T)/6–311+G(d,p)+ZPE levels of theory at 0 K and the CBS energies with ZPE corrected are given in the parentheses. [Color figure can be viewed in the online issue, which is available at wileyonlinelibrary.com.]

Table 1. Relative energies[a] (kcal/mol) of various species at 0 K in the Si_2H_5 thermal decomposition reaction calculated at the different levels.

Species	B3LYP/6–311++G(3df,2p)	CCSD(T)/6–311+G(d,p)	CCSD(T)/6–311++G(3df,2p)// CCSD(T)/6–311+G(d,p)	CBS//CCSD(T)/6–311+G(d,p)
$^2Si_2H_5$	0.0	0.0	0.0	0.0
^{2}TS1	27.3 (28.2[b])	30.8	29.6 (29.0[c])	29.3
^{2}TS2	31.9	35.4	33.4	33.5
^{2}LM1($SiH\cdots SiH_4$)	30.7 (31.7[b])	31.7	31.8 (31.2[c])	33.2
$^2SiH + {}^1SiH_4$	37.6 (37.1[b])	36.4	38.5 (39.0[c])	41.4
^{2}TS3	35.3	39.1	37.3	36.9
^{2}TS4	49.1	53.4	50.9	50.7
^{2}TS5	45.8	44.5	43.0	43.2
$^2H_2SiSiH + {}^1H_2$	37.6	41.1	38.8	41.4
$^2SiH_3 + {}^1SiH_2$	52.1 (51.8[b])	51.6	53.4 (53.8[c])	56.0
$^1Si_2H_4(C_{2h}) + {}^2H$	64.7	61.4	61.4	63.3

[a] Energies are ZPE corrected. [b] Evaluated with B3LYP/6–311G(d,p) from Ref. [12]. [c] Evaluated with CCSD(T)/aug-cc-pVTZ from Ref. [12]

Results and Discussions

Potential energy surfaces and reaction mechanisms

In this section, the Si_2H_5 thermal decomposition is investigated for formation of smaller silicon hydrides, specifically, SiH, SiH_2, SiH_3, SiH_4, $HSiSiH_2$, and Si_2H_4. The geometric parameters of reactants, intermediates, and TSs optimized at the CCSD(T)/6–311+G(d,p) level are given in Figure 1. The potential energy diagram of Si_2H_5 of the fragmentation pathways using the refined energies predicted with the CCSD(T)/6–311++G(3df,2p)//CCSD(T)/6–311+G(d,p) method is presented in Figure 2. The relative energies of the stationary points obtained from different calculations are summarized in Table 1. In the following discussion, the extrapolated CBS energies are given in the accompanied parentheses for comparison; with the exception of a few cases, most values obtained by the two methods agree within 1 kcal/mol. The rotational constants and vibrational frequencies for all of the stationary points computed at the CCSD(T)/6–311+G(d,p) level are summarized in Table 2.

According to the CCSD(T)/6–311++G(3df,2p)//CCSD(T)/6–311+G(d,p) calculations, the lowest energy pathway for Si_2H_5 fragmentation is the migration of one hydrogen atom from the SiH_2-moiety of the H_2Si-SiH_3 structure to the SiH_3 moiety via the mono-hydrogen-bridged structure $HSiHSiH_3$ at TS2 with a barrier height of 33.4 (33.5) kcal/mol. The production of the $SiH + SiH_4$ products occurs via the hydrogen-bridged complex, $SiH\cdots SiH_4$ (local minimal 1, LM1) locating at −1.6 (−0.3) kcal/mol relative to TS2. The decomposition reaction is endothermic by 38.8 (41.4) kcal/mol. Another pathway for the fragmentation leading to the same products via LM1 is the simultaneous migration of two H-atoms from the SiH_3 moiety to the SiH_2 via TS5 with an energy barrier of 43.0 (43.2) kcal/mol.

Aside from the production of the $SiH + SiH_4$ product pair, the disilanyl radical can also decompose by elimination of a hydrogen atom and a hydrogen molecule. The pathway of H_2 elimination can take place from the SiH_3 moiety, proceeding over the saddle point at TS4 which has the characteristic H···H bond length of 1.073 Å and a barrier height of 50.9 (50.7) kcal/mol. The elimination of the H-atom from Si_2H_5, however, is a barrierless dissociation process producing Si_2H_4 (C_{2h}) with the largest endothermicity of 61.4 (63.3) kcal/mol relative to Si_2H_5. Si_2H_5 can also decompose by breaking the Si—Si bond

Table 2. Vibrational frequencies and rotational constants for the various stationary points of the Si_2H_5 thermal decomposition reaction at the CCSD (T)/6–311+G(d,p) level of theory.

Species	A (GHz)	B (GHz)	C (GHz)	Frequencies (cm^{-1})
^{2}SiH		224.1		2064
$^1SiH_2$	244.1	209.1	112.6	1042, 2094, 2098
$^2SiH_3$	142.4	142.4	84.2	801, 957, 957, 2259, 2293, 2293
$^1SiH_4$	86.1	86.1	86.1	955, 955, 955, 991, 991, 2291, 2296, 2296, 2296
$^2HSiSiH_2$	96.0	6.1	5.8	189, 391, 419, 471, 689, 979, 2095, 2242, 2267
$^1Si_2H_4(C_{2h})$	74.2	6.2	5.9	347, 414, 447, 516, 561, 634, 939, 966, 2268, 2273, 2287, 2297
$^2Si_2H_5$	53.5	5.3	5.2	144, 404, 432, 444, 623, 655, 905, 955, 968, 970, 2246, 2256, 2268, 2272, 2280 (127, 390, 405, 424, 596, 637, 875, 936, 949, 950, 2188, 2199, 2213, 2223, 2231)[12]
^{2}LM1($SiH\cdots SiH_4$)	63.7	3.6	3.6	83, 138, 257, 454, 685, 804, 922, 957, 973, 1260, 1934, 2039, 2298, 2328, 2344 (31, 131, 234, 439, 648, 754, 887, 936, 957, 1209, 1829, 1988, 2242, 2275, 2291)[12]
^{2}TS1	58.3	5.5	5.3	*i*207, 112, 340, 424, 701, 713, 900, 921, 929, 1310, 1545, 2220, 2225, 2249, 2261 (*i*225, 128, 333, 400, 676, 705, 885, 904, 916, 1240, 1503, 2160, 2161, 2190, 2205)[12]
^{2}TS2	54.3	5.1	5.0	*i*468, 212, 374, 442, 659, 760, 924, 950, 988, 1017, 1703, 2121, 2210, 2280, 2312
^{2}TS3	56.7	5.6	5.4	*i*903, 275, 417, 423, 549, 658, 667, 887, 938, 962, 1487, 2199, 2256, 2278, 2291
^{2}TS4	49.4	5.5	5.3	*i*1160, 140, 303, 429, 455, 630, 691, 807, 927, 1013, 1668, 2074, 2224, 2234, 2249
^{2}TS5	63.38	4.69	4.57	*i*891, 289, 369, 449, 494, 718, 880, 929, 958, 1302, 1502, 1858, 2080, 2283, 2325

Table 3. Enthalpies of formation ($\Delta_f H^\circ$) of species at 0 K predicted at the CCSD(T)/6–311++G(3df,2p)//CCSD(T)/6–311+G(d,p)+ZPE level of theory. The CBS energies with ZPE corrected are listed in the parentheses.

		Enthalpy of formation $\Delta_f H_0^\circ$ (kcal/mol)	
Species	Reactions	Calculated	Literatures
^2SiH	$^2Si_2H_5 \rightarrow {}^1SiH_4 + {}^2SiH$	87.2 (90.0)	89.6 ± 2.0[25]
$^1SiH_2$	$^2Si_2H_5 \rightarrow {}^1SiH_2 + {}^2SiH_3$	64.9 (67.5)	65.5 ± 0.7[29]
$^2HSiSiH_2$	$^2Si_2H_5 \rightarrow {}^2HSiSiH_2 + {}^1H_2$	98.0 (100.6)	98.8[30]
	$^2HSiSiH_2 + {}^1C_2H_6 \rightarrow {}^1Si_2H_6 \rightarrow {}^2HCCH_2$	97.3 (99.6)	
$^1Si_2H_4(C_{2h})$	$^2Si_2H_5 \rightarrow {}^2H + {}^1Si_2H_4$	68.9 (70.9)	67.9 ± 0.9[11]
	$^1Si_2H_4 + {}^1C_2H_6 \rightarrow {}^1Si_2H_6 + {}^1C_2H_4$	69.4 (71.1)	69.32; 68.84[31]
			66.5[30]

The experimental values are obtained based on the enthalpies of formation at 0 K for H = 51.66 kcal/mol[25]; H_2 = 0.0 kcal/mol[25]; $HCCH_2$ = 71.5 kcal/mol[32]; C_2H_4 =14.6 kcal/mol[25]; C_2H_6 = −16.3 kcal/mol[33]; SiH = 89.6 kcal/mol[25]; SiH_2 = 65.5 kcal/mol[29]; SiH_3 = 47.7 ± 1.2 kcal/mol[34]; SiH_4 = 10.5 kcal/mol[25]; Si_2H_4 = 67.9 kcal/mol[11]; Si_2H_5 = 59.2 kcal/mol[11]; and Si_2H_6 = 22.9 kcal/mol[11].

to produce SiH_2 and SiH_3 with an endothermicity of 53.4 (56.0) kcal/mol; the reaction also occurs barrierlessly without an intrinsic TS. Additionally, there are two TSs of H-shift, TS1 and TS3, from the SiH_3 moiety both having a bridged H-atom with C_1 symmetry giving rise to the same Si_2H_5 structure after rearrangement with noticeably different barriers of 29.6 (29.3) and 37.3 (36.9) kcal/mol.

The above results for the SiH···SiH_4 complex (LM1), $SiH + SiH_4$, $SiH_2 + SiH_3$, and $H_2SiHSiH_2$ (TS1) obtained at the higher levels of theory in the present work are in good agreement with previous estimates of 31.2, 39.0, 53.8, and 29.0 kcal/mol relative to Si_2H_5, respectively, by Sillars et al. with the CCSD(T)/aug-cc-pVTZ//B3LYP/6–311G(d,p) method.[12] It should be mentioned that aside from the TSs described above, we have also searched at length, but to no avail, for the existence of a roaming transition state in the bimolecular metathetical process $SiH + SiH_4 \iff SiH_3 + SiH_2$ at a long separation.

Enthalpies of the formation

For the purpose of validating the relative energies for prediction of rate coefficients, we compare the enthalpies of formation $\Delta_f H^\circ$ of some compounds with those of available experimental results based on the calculated enthalpies of the reaction $\Delta_r H^\circ$ at 0 K. Furthermore, isodesmic reactions are also used to examine the calculated enthalpies of formation at 0 K, such as $^1Si_2H_4 + {}^1C_2H_6 \rightarrow {}^1Si_2H_6 + {}^1C_2H_4$ and $^2HSiSiH_2 + {}^1C_2H_6 \rightarrow {}^1Si_2H_6 + {}^2HCCH_2$. The predicted enthalpies of formation, including ^2SiH, $^1SiH_2$, $HSiSiH_2$, and $Si_2H_4(C_{2h})$ are presented in Table 3, which are derived by the above calculated enthalpies of reaction at the CCSD(T)/6–311++G(3df,2p)//CCSD(T)/6–311+G(d,p) level with published values of $\Delta_f H^\circ$ (0 K) from the NIST-JANAF Tables[25] and the relevant literature.[11,29–34] For instance, $\Delta_f H^\circ$ (0 K) for $Si_2H_4(C_{2h})$ could be obtained from the equation as follows,

$$\Delta_f H^\circ(Si_2H_4) = \Delta_f H^\circ(Si_2H_5) - \Delta_f H^\circ(H) + \Delta_r H^\circ, \text{ at 0 K.} \quad (11)$$

These $\Delta_f H^\circ$ (0 K) results of ^2SiH, $^1SiH_2$, $^2HSiSiH_2$, and $^1Si_2H_4(C_{2h})$ using $\Delta_r H^\circ$ (0 K) relevant to Si_2H_5 decomposition reactions are 87.2, 64.9, 98.0, and 68.9 kcal/mol, respectively. In addition, $\Delta_f H^\circ$ (0 K) results of $^2HSiSiH_2$ and $^1Si_2H_4(C_{2h})$ using $\Delta_r H^\circ$ (0 K) of isodesmic reactions are 97.3 and 69.4 kcal/mol, respectively. These agree reasonably well with the reported findings of ^2SiH (89.6 ± 2.0 kcal/mol, NIST[25]), $^1SiH_2$ (65.5 ± 0.7 kcal/mol, Berkowitz et al.[29]), $^2HSiSiH_2$ (98.8 kcal/mol, Curtiss et al.[30]), and $^1Si_2H_4$ (67.9 ± 0.9, Ruscic and Berkowitz.[11]).

Rate constant calculations

The present theoretical predictions of rate constants for the reactions were carried out with CVTST by searching for the position of the dividing surface with a maximum ΔG° ($T,s = s^\ddagger$) for a barrierless process, specifically $Si_2H_5 \leftrightarrows Si_2H_4(C_{2h}) + H$, $Si_2H_5 \leftrightarrows SiH_3 + SiH_2$ and the dissociation of LM1 to $SiH + SiH_4$. To reduce the computational expense, the MEPs are computed using the potential energies along the reaction coordinate (Si···H) from about 1.5 to 5.5 Å with a step size 0.2 Å in $Si_2H_5 \leftrightarrows Si_2H_4(C_{2h}) + H$ and the reaction coordinate (Si···Si) from about 2.4 to 5.0 Å with a step size 0.2 Å in $Si_2H_5 \leftrightarrows SiH_3 + SiH_2$ at the UB3LYP/6–311++G(3df,2p) level combined with the cubic spline interpolation method[35] and the energy is scaled at the CCSD(T)/6–311++G(3df,2p)+ZPE level. The approximate positions of the dividing surface for the barrierless reactions are estimated in Table 4. Furthermore, rate constants of RRKM calculations are based on CCSD(T)/6–311++G(3df,2p)//CCSD(T)/6–311+G(d,p) energies. The MEP for the dissociation of LM1($SiH\cdots SiH_4$) $\rightarrow SiH + SiH_4$ followed by a similar search can be represented by the Morse potential, $V(r) = D_e\{1 - \exp[-\beta_e(r - r_e)]\}^2$ according to the B3LYP/6–311++G(3df,2p) calculations with the energy scaled at the CCSD(T)/6–311++G(3df,2p)+ZPE level, and obtained parameters of D_e = 6.76 kcal/mol, β_e = 2.311 $Å^{-1}$, and r_e = 1.8 Å. The effective sum of states for all of the TSs is estimated at the energy E and total angular momentum J resolved level using rigid-rotor harmonic oscillator assumptions for the energy

Table 4. The estimated corresponding position of the dividing surface by CVTST method.

$^2Si_2H_5 \leftrightarrows {}^1Si_2H_4\ (C_{2h}) + {}^2H$							
T (K)	300–500	600–900	1000–1100	1200	1300–1500	1600–1700	1800–2000
Si···H (Å)	3.45	3.25	3.15	3.1	3.05	3.0	2.95
$^2Si_2H_5 \leftrightarrows {}^1SiH_2 + {}^2SiH_3$							
T (K)	300–600	700–1000	1100–1400	1500–1800	1900–2000		
Si···Si (Å)	4.15	4.05	3.9	3.75	3.65		

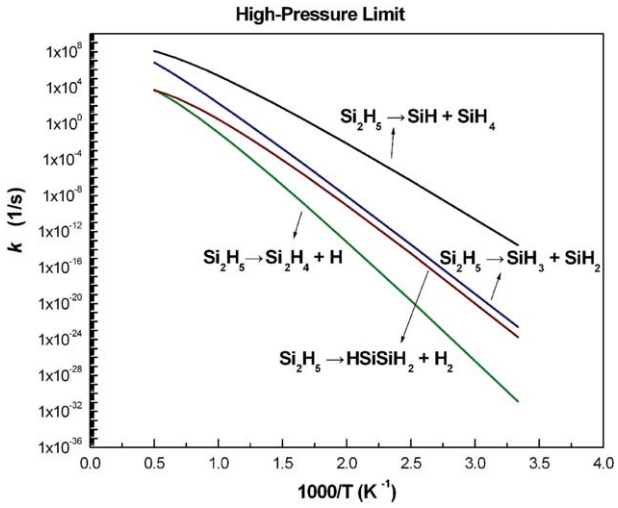

Figure 3. Comparisons of high-pressure limit rate constants between $^2Si_2H_5 \rightarrow {}^1Si_2H_4$ (C_{2h}) + ^2H (green —), $^2Si_2H_5 \rightarrow {}^2SiH_3 + {}^1SiH_2$ → (blue —), $^2Si_2H_5 \rightarrow {}^2HSiSiH_2 + {}^1H_2$ (brown —), and $^2Si_2H_5 \rightarrow {}^2SiH + {}^1SiH_4$ (black —) versus the inverse of temperature. [Color figure can be viewed in the online issue, which is available at wileyonlinelibrary.com.]

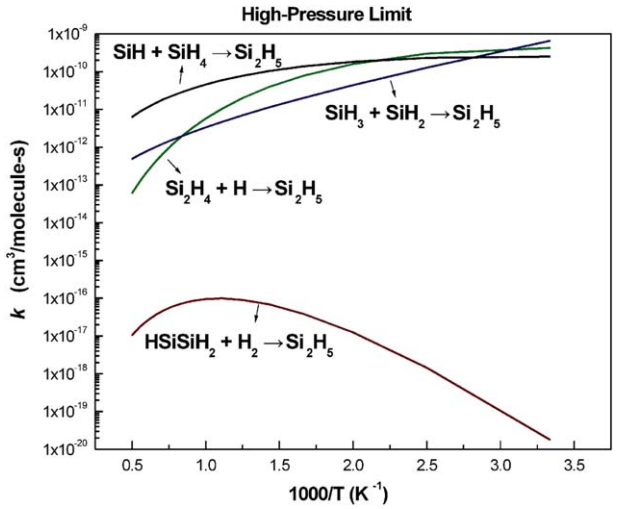

Figure 4. Comparisons of high-pressure limit rate constants between $^1Si_2H_4$ (C_{2h}) + ^2H → $^2Si_2H_5$ (green —), $^2SiH_3 + {}^1SiH_2$ → $^2Si_2H_5$ (blue —), $^2HSiSiH_2 + {}^1H_2$ → $^2Si_2H_5$ (brown —), and $^2SiH + {}^1SiH_4$ → $^2Si_2H_5$ (black —) versus the inverse of temperature. [Color figure can be viewed in the online issue, which is available at wileyonlinelibrary.com.]

levels. The $\langle \Delta E_{down} \rangle$ is assumed to be equal to 400 cm^{-1}. The parameters for the Lennard–Jones collision rate were approximated by $\sigma = 4.717$ Å and $\varepsilon = 213.2$ cm^{-1} for Si_2H_5[36] and $\sigma = 3.75$ Å and $\varepsilon = 98.3$ cm^{-1} for Ar[37].

Unimolecular Decomposition of Si_2H_5. The PES shown in Figure 2 indicates that the unimolecular decomposition of Si_2H_5 radical may produce SiH + SiH_4, $H_2SiSiH + H_2$, $SiH_2 + SiH_3$, and Si_2H_4 (C_{2h}) + H:

$$Si_2H_5 \rightarrow SiH + SiH_4 \quad (1)$$
$$\rightarrow HSiSiH_2 + H_2 \quad (2)$$
$$\rightarrow SiH_3 + SiH_2 \quad (3)$$
$$\rightarrow Si_2H_4(C_{2h}) + H \quad (4)$$

Interestingly, the last product pair is most endothermic, contrary to the decomposition of C_2H_5 which produces exclusively C_2H_4 + H because of the strong Π-bond energy in ethylene.[38] In the present case, the production of SiH + SiH_4, reaction Eq. (1), via TS2 (33.4 kcal/mol) and the product pair complex LM1 (31.8 kcal/mol), with 38.8 kcal/mol endothermicity, is most favorable. The dehydrogenation process, reaction Eq. (2), giving H_2SiSiH takes place via TS4 with a barrier of 50.9 kcal/mol and is endothermic by 38.8 kcal/mol, the same as that of the SiH + SiH_4 reaction. However, the much higher barrier for the dehydrogenation step makes the process less competitive as one would expect. Similarly reactions Eqs. (3) and (4) with higher endothermicities producing $SiH_2 + SiH_3$ (53.4 kcal/mol) and Si_2H_4 (C_{2h}) + H (61.4 kcal/mol), both predicted to occur without well-defined intrinsic barriers as aforementioned, are expected to be too slow to compete with the most favored process also. The high-pressure limits for the decomposition and the related reverse association reactions are shown in Figures 3 and 4, respectively, for comparison. Their relative importance in the decomposition reactions mainly reflects the enthalpy of activation controlled by the corresponding VTS's for radical production and the TS for H_2 elimination. The formation of Si_2H_5 from the recombination processes under the high-pressure condition (Fig. 4) reflects the nature of the interaction between the reaction pair and the entropic changes at VTS's along the MEP at large separations. It should be noted that the negative temperature dependence of the rate constant for $HSiSiH_2 + H_2$ reaction at high temperatures can be attributed largely to the $T^{-3/2}$-factor deriving from the rotational and translational partition function ratios of the TS and the reactants.

The least-squares-fitted three-parameter rate constants predicted for various pressures for the temperature range 300–1000 K are summarized in Tables 5 and 6 for kinetic modeling applications.

Related Bimolecular Reactions Involving Si_2H_5 as Intermediate. Under PECVD conditions using SiH_4 as the precursor, SiH_x ($x = 1-3$) and the two isomers of Si_2H_4 may coexist in the gas phase. We have thus also evaluated the rate constants for the bimolecular processes involving these species in conjunction with Si_2H_5 as the intermediate as fully characterized by the PES shown in Figure 2. The mechanisms of these bimolecular reactions giving the most favorable products are described as follows:

i. $^2SiH + {}^1SiH_4$ reactions:

$$^2SiH + {}^1SiH_4 \leftrightarrow {}^2Si_2H_5^* \rightarrow {}^2SiH_3 + {}^1SiH_2$$
$$\downarrow$$
$$^2Si_2H_5$$

ii. $^2HSiSiH_2 + {}^1H_2$ reactions:

$$^2HSiSiH_2 + {}^1H_2 \leftrightarrow {}^2Si_2H_5^* \rightarrow {}^2SiH + {}^1SiH_4$$
$$\downarrow$$
$$^2Si_2H_5$$

Table 5. Arrhenius parameters[a] including high-pressure limit (k_∞) and low-pressure limit (k_0) for the $^2Si_2H_5 \rightarrow {}^2SiH + {}^1SiH_4$ and $^2Si_2H_5 \rightarrow {}^2HSiSiH_2 + {}^1H_2$ reactions.

	P (Torr)	A	n	E_a/R (K)	T range (K)
$^2Si_2H_5 \rightarrow {}^2SiH + {}^1SiH_4$					
k_∞	∞	4.98×10^{35}	−6.92	22146.7	300–2000
k_0	–	2.52×10^{33}	−10.21	21795.7	300–2000
k	0.3	2.21×10^{43}	−10.35	22101.3	300–2000
k	0.4	3.32×10^{43}	−10.36	22135.3	300–2000
k	0.5	4.41×10^{43}	−10.37	22160.5	300–2000
k	0.6	5.65×10^{43}	−10.38	22184.0	300–2000
k	1	1.17×10^{44}	−10.40	22261.0	300–2000
k	10	1.78×10^{45}	−10.45	22721.0	300–2000
k	760	1.12×10^{42}	−9.02	22932.8	300–2000
$^2Si_2H_5 \rightarrow {}^2HSiSiH_2 + {}^1H_2$					
k_∞	∞	3.38×10^{44}	−10.44	29284.9	300–2000
k_0	–	6.04×10^{19}	−8.79	25005.2	300–2000
k	0.3	6.39×10^{30}	−9.19	25121.5	300–2000
k	0.4	1.63×10^{31}	−9.26	25150.3	300–2000
k	0.5	3.69×10^{31}	−9.33	25177.5	300–2000
k	0.6	7.90×10^{31}	−9.40	25208.3	300–2000
k	1	8.11×10^{32}	−9.60	25305.8	300–2000
k	10	2.67×10^{40}	−11.27	26419.5	300–2000
k	760	3.27×10^{51}	−13.04	29736.6	300–2000

[a] $k(T) = AT^n\exp(-E_a/RT)$. Unit of the rate constants $k(T)$ is (s^{-1}) and k_0 is (cm^3 $molecule^{-1}$ s^{-1}).

iii. $^2SiH_3 + {}^1SiH_2$ reactions:

$$^2SiH_3 + {}^1SiH_2 \leftrightarrow {}^2Si_2H_5^* \rightarrow {}^2SiH + {}^1SiH_4$$
$$\downarrow$$
$$^2Si_2H_5$$

Table 6. Arrhenius parameters[a] including high-pressure limit (k_∞) and low-pressure limit (k_0) for the $^2Si_2H_5 \rightarrow {}^1Si_2H_4$ (C_{2h}) + ^2H and $^2Si_2H_5 \rightarrow {}^1SiH_2 + {}^2SiH_3$ reactions.

	P (Torr)	A	n	E_a/R (K)	T range (K)
$^2Si_2H_5 \rightarrow {}^1SiH_2 + {}^2SiH_3$					
k_∞	∞	4.76×10^{26}	−4.26	26741.9	300–2000
k_0	–	4.15×10^{-6}	0.15	23615.3	300–2000
k	0.3	1.12×10^{5}	−0.09	23476.1	300–2000
k	0.4	2.27×10^{5}	−0.14	23459.1	300–2000
k	0.5	4.21×10^{5}	−0.18	23448.9	300–2000
k	0.6	6.86×10^{5}	−0.22	23434.5	300–2000
k	1	3.71×10^{6}	−0.35	23408.7	300–2000
k	10	6.44×10^{12}	−1.71	23686.6	300–2000
k	760	8.85×10^{29}	−5.60	26818.0	300–2000
$^2Si_2H_5 \rightarrow {}^1Si_2H_4$ (C_{2h}) + ^2H					
k_∞	∞	6.58×10^{39}	−8.68	33992.1	300–2000
k_0	–	3.23×10^{14}	−6.36	32558.9	300–2000
k	0.3	7.99×10^{23}	−6.36	32504.3	300–2000
k	0.4	1.12×10^{24}	−6.36	32478.9	300–2000
k	0.5	1.52×10^{24}	−6.37	32459.7	300–2000
k	0.6	1.89×10^{24}	−6.37	32440.4	300–2000
k	1	4.10×10^{24}	−6.40	32389.8	300–2000
k	10	8.63×10^{26}	−6.73	32112.8	300–2000
k	760	4.52×10^{38}	−9.08	33070.4	300–2000

[a] $k(T) = AT^n\exp(-E_a/RT)$. Unit of the rate constants $k(T)$ is (s^{-1}) and k_0 is (cm^3 $molecule^{-1}$ s^{-1}).

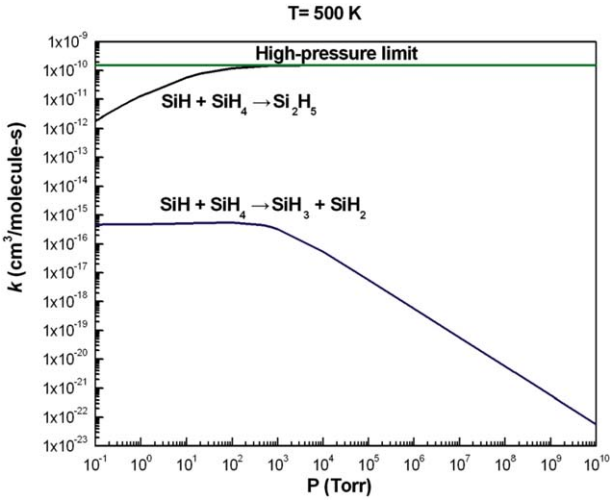

Figure 5. Predicted rate constants as a function of pressure at $T = 500$ K for $^2SiH + {}^1SiH_4 \rightarrow {}^2Si_2H_5$ and $^2SiH + {}^1SiH_4 \rightarrow {}^2SiH_3 + {}^1SiH_2$. [Color figure can be viewed in the online issue, which is available at wileyonlinelibrary.com.]

iv. $^1Si_2H_4(C_{2h}) + {}^2H$ reactions:

$$^1Si_2H_4(C_{2h}) + {}^2H \leftrightarrow {}^2Si_2H_5^* \rightarrow {}^2SiH + {}^1SiH_4$$
$$\downarrow$$
$$^2Si_2H_5$$

For these bimolecular reactions, the predicted rate constants for energetically most favorable product channels as a function of pressure at $T = 500$ K and the temperature dependence at different pressures are graphically presented as follows: Reaction I in Figures 5–7; reaction II in Figures 8–10; reaction III in Figures 11–13; and reaction IV in Figures 14–16. All the processes involved in the decomposition and the reverse association reactions are highly pressure dependent due to the small size of the system and the associated high energy changes. For the convenience of modeling application, the three

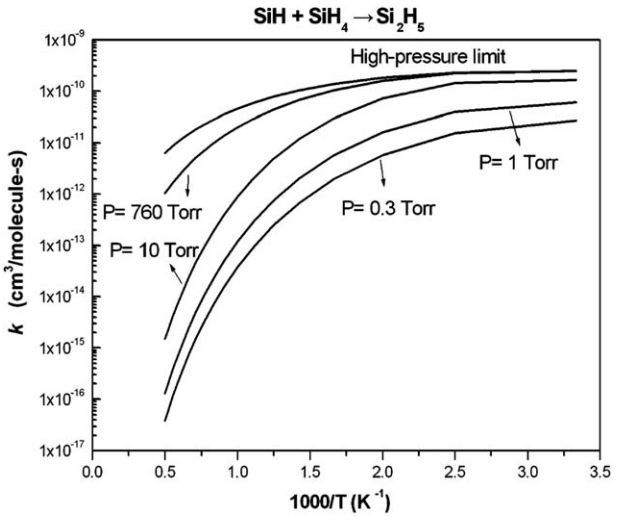

Figure 6. Arrhenius plots of rate constants for $^2SiH + {}^1SiH_4 \rightarrow {}^2Si_2H_5$ at different pressures as labeled versus the inverse of temperature.

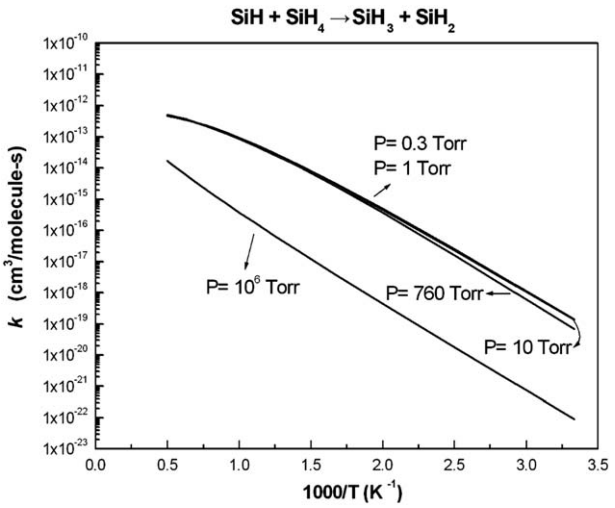

Figure 7. Arrhenius plots of rate constants for $^2SiH + {}^1SiH_4 \rightarrow {}^2SiH_3 + {}^1SiH_2$ at different pressures as labeled versus the inverse of temperature.

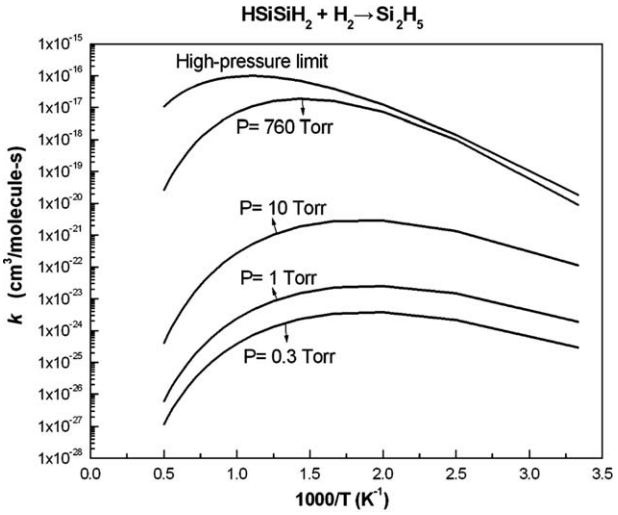

Figure 9. Arrhenius plots of rate constants for $^2HSiSiH_2 + {}^1H_2 \rightarrow {}^2Si_2H_5$ at different pressures as labeled versus the inverse of temperature.

parameter equations for the modified Arrhenius expressions in the temperature range of 300−2000 K at various pressures are presented in Table 7 (for reaction I), Table 8 (for reaction II), Table 9 (for reaction III), and Table 10 (for reaction IV).

The predicted results show that in reactions (II)–(IV), products such as $SiH + SiH_4$ are dominant at low pressure, while the stabilized adduct Si_2H_5 becomes gradually prevalent as the pressure increases. The other product pairs ($SiH_3 + SiH_2$, Si_2H_4 (C_{2h}) + H, and $HSiSiH_2 + H_2$) are energetically inaccessible from $SiH + SiH_4$. At room temperature and low pressure of silicon CVD environments, the reaction of $SiH + SiH_4$ to produce Si_2H_5 is predominant, followed in order by $SiH_3 + SiH_2$, Si_2H_4 (C_{2h}) + H, and $HSiSiH_2 + H_2$. The predicted rate constant for $SiH + SiH_4$ at 500 K in the low pressure (∼mTorr) range is in close agreement with the estimate of Jasinski et al.,[4] on the order of 10^{-12} cm^3 $molecule^{-1}$ s^{-1}. For these bimolecular and the unimolecular dissociation of Si_2H_5, their high-pressure limit rate constants as presented before in Figures 3 and 4, respectively, clearly depict their relative importance.

Concluding Remarks

In the present work, we have investigated the fundamental reactions relevant to the thermal decomposition of Si_2H_5 radical and its related reverse bimolecular reactions with *ab initio* MO calculations based on the B3LYP/6–311++G(3df,2p), CCSD(T)/6–311++G(3df,2p)//CCSD(T)/6–311+G(d,p), and CCSD(T)/6–311+G(d,p)//CBS methods. Based on the predicted values at the CCSD(T)/6–311++G(3df,2p)//CCSD(T)/6–311+G(d,p) level, the lowest energy path leads to the production of SiH and SiH_4 via a transition state (TS2) with a barrier height of 33.4 kcal/mol relative to Si_2H_5. Additionally, to break the H—SiH_2 and Si—Si bonds require 61.4 and 53.4 kcal/mol, respectively. Furthermore, the enthalpies of the formation $\Delta_f H^\circ$ for the major products at 0 K have been predicted using the

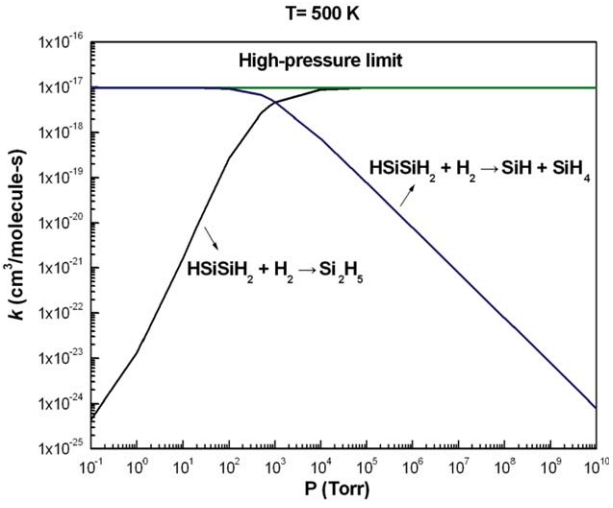

Figure 8. Predicted rate constants as a function of pressure at $T = 500$ K for $^2HSiSiH_2 + {}^1H_2 \rightarrow {}^2Si_2H_5$ and $^2HSiSiH_2 + {}^1H_2 \rightarrow {}^2SiH + {}^1SiH_4$. [Color figure can be viewed in the online issue, which is available at wileyonlinelibrary.com.]

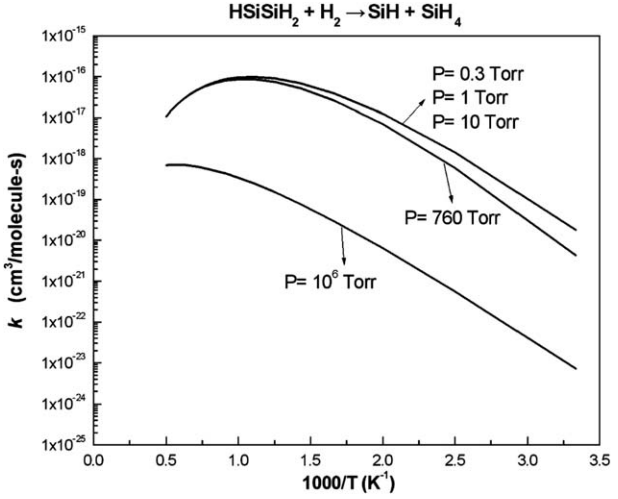

Figure 10. Arrhenius plots of rate constants for $^2HSiSiH_2 + {}^1H_2 \rightarrow {}^2SiH + {}^1SiH_4$ at different pressures as labeled versus the inverse of temperature.

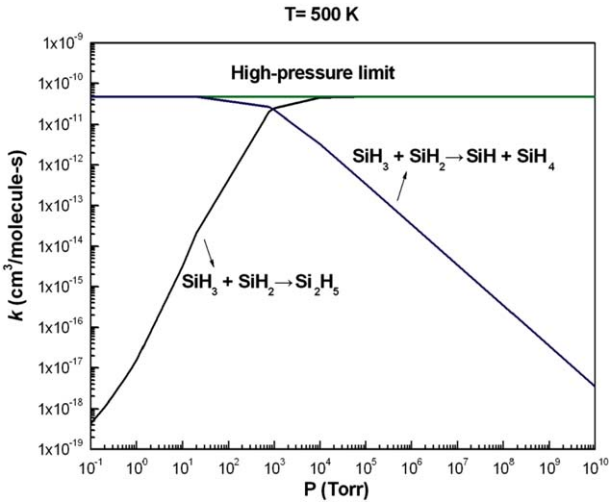

Figure 11. Predicted rate constants as a function of pressure at $T = 500$ K for $^2SiH_3 + {}^1SiH_2 \rightarrow {}^2Si_2H_5$ and $^2SiH_3 + {}^1SiH_2 \rightarrow {}^2SiH + {}^1SiH_4$. [Color figure can be viewed in the online issue, which is available at wileyonlinelibrary.com.]

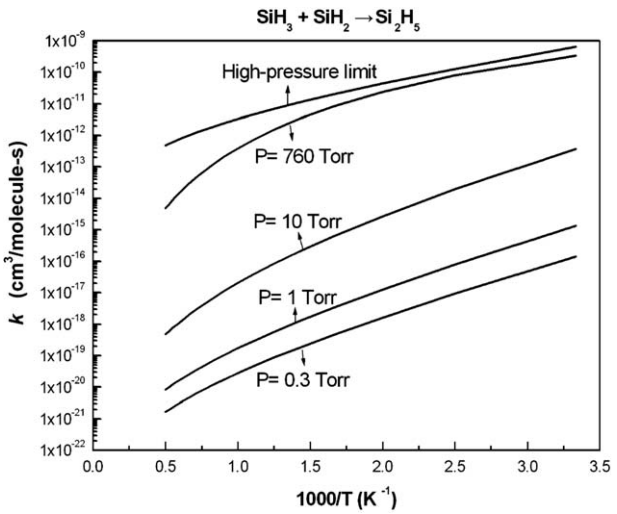

Figure 12. Arrhenius plots of rate constants for $^2SiH_3 + {}^1SiH_2 \rightarrow {}^2Si_2H_5$ at different pressures as labeled versus the inverse of temperature.

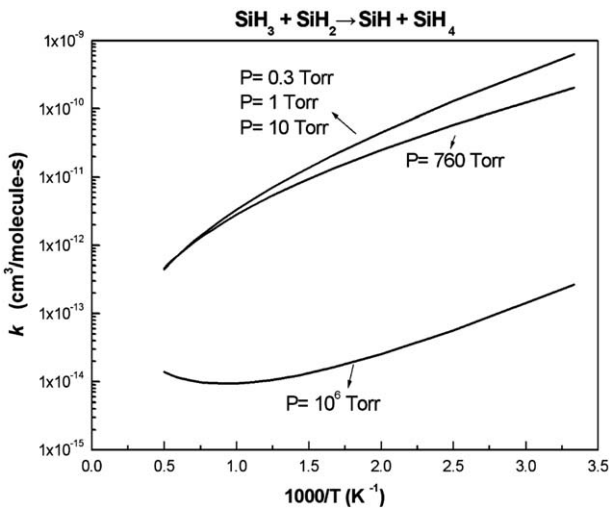

Figure 13. Arrhenius plots of rate constants for $^2SiH_3 + {}^1SiH_2 \rightarrow {}^2SiH + {}^1SiH_4$ at different pressures as labeled versus the inverse of temperature.

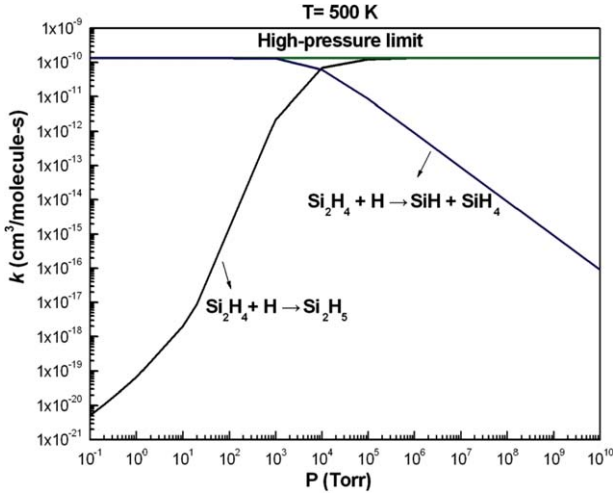

Figure 14. Predicted rate constants as a function of pressure at $T = 500$ K for $^1Si_2H_4$ (C_{2h}) + $^2H \rightarrow {}^2Si_2H_5$ and $^1Si_2H_4$ (C_{2h}) + $^2H \rightarrow {}^2SiH + {}^1SiH_4$. [Color figure can be viewed in the online issue, which is available at wileyonlinelibrary.com.]

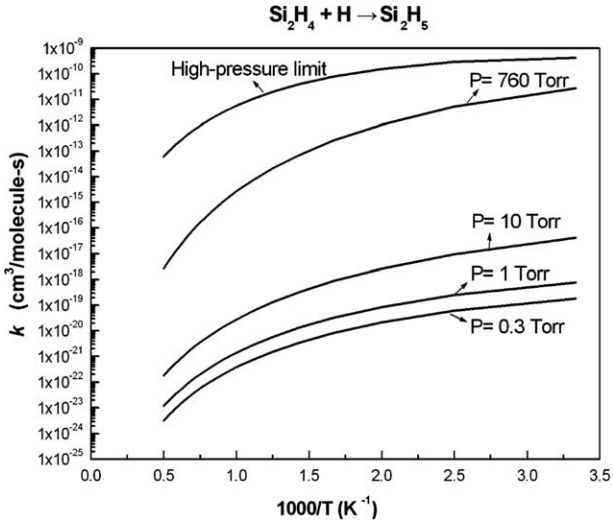

Figure 15. Arrhenius plots of rate constants for $^1Si_2H_4$ (C_{2h}) + $^2H \rightarrow {}^2Si_2H_5$ at different pressures as labeled versus the inverse of temperature.

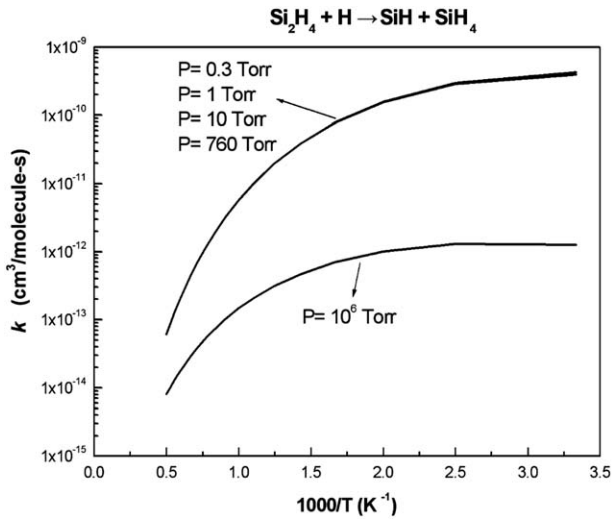

Figure 16. Arrhenius plots of rate constants for $^1Si_2H_4$ (C_{2h}) + $^2H \rightarrow {}^2SiH + {}^1SiH_4$ at different pressures as labeled versus the inverse of temperature.

Table 7. Arrhenius parameters[a] including high-pressure limit (k_∞) and low-pressure limit (k_0) for the $^2SiH + {}^1SiH_4 \rightarrow {}^2Si_2H_5$ and $^2SiH + {}^1SiH_4 \rightarrow {}^1SiH_2 + {}^2SiH_3$ reactions.

	P (Torr)	A	*n*	E_a/R (K)	*T* range (K)
$^2SiH + {}^1SiH_4 \rightarrow {}^2Si_2H_5$					
k_∞	∞	1.89×10^{1}	−3.70	1184.0	300–2000
k_0	–	4.02×10^{15}	−12.35	3270.2	300–2000
k	0.3	5.72×10^{25}	−12.53	3644.3	300–2000
k	0.4	8.54×10^{25}	−12.55	3680.4	300–2000
k	0.5	1.20×10^{26}	−12.56	3714.0	300–2000
k	0.6	1.56×10^{26}	−12.57	3740.7	300–2000
k	1	3.55×10^{26}	−12.60	3833.4	300–2000
k	10	1.05×10^{26}	−12.11	4006.7	300–2000
k	760	5.35×10^{6}	−5.55	1785.0	300–2000
$^2SiH + {}^1SiH_4 \rightarrow {}^1SiH_2 + {}^2SiH_3$					
k	10^6	2.62×10^{-17}	1.24	5890.2	300–2000
k	low P∼1	6.75×10^{-3}	−2.61	7071.6	300–2000
k	10	9.57×10^{-2}	−2.95	7270.9	300–2000
k	760	6.47×10^{-1}	−3.17	7681.8	300–2000

[a] $k(T) = AT^n\exp(-E_a/RT)$. Unit of the rate constants $k(T)$ is (cm^3 $molecule^{-1}$ s^{-1}) and k_0 is (cm^6 $molecule^{-2}$ s^{-1}).

computed enthalpies of the reaction $\Delta_r H^\circ$ at 0 K, including the isodesmic reactions at this level. The results are in reasonable agreement with previous experimental values, for example, SiH (87.2 kcal/mol), SiH_2 (64.9 kcal/mol), $HSiSiH_2$ (98.0 kcal/mol), and Si_2H_4 (68.9 kcal/mol). Finally, the rate constants for Si_2H_5 decomposition into these smaller silicon hydrides and their corresponding reverse reactions via the disilanyl intermediate have been calculated using the variational RRKM theory by solving the master equation. The results indicate that the formation of the energetically most favored products $SiH + SiH_4$ is predominant under varying P, T conditions. The rate constants predicted under different practically accessible conditions have been evaluated and tabulated for future modeling and optimization of homogenous a-Si:H film growth on large-area substrates.

Table 8. Arrhenius parameters[a] including high-pressure limit (k_∞) and low-pressure limit (k_0) for the $^1SiH_2 + {}^2SiH_3 \rightarrow {}^2Si_2H_5$ and $^1SiH_2 + {}^2SiH_3 \rightarrow {}^2SiH + {}^1SiH_4$ reactions.

	P (Torr)	A	*n*	E_a/R (K)	*T* range (K)
$^1SiH_2 + {}^2SiH_3 \rightarrow {}^2Si_2H_5$					
k_∞	∞	2.17×10^{-7}	−1.80	−1330.4	300–2000
k_0	–	5.78×10^{-25}	−2.04	−2367.0	300–2000
k	0.3	1.63×10^{-14}	−2.28	−2481.3	300–2000
k	0.4	3.45×10^{-14}	−2.33	−2490.4	300–2000
k	0.5	6.00×10^{-14}	−2.37	−2505.2	300–2000
k	0.6	1.01×10^{-13}	−2.40	−2514.9	300–2000
k	1	5.32×10^{-13}	−2.53	−2536.1	300–2000
k	10	7.29×10^{-7}	−3.84	−2224.6	300–2000
k	760	1.88×10^{8}	−6.80	624.4	300–2000
$^1SiH_2 + {}^2SiH_3 \rightarrow {}^2SiH + {}^1SiH_4$					
k	10^6	1.61×10^{-23}	2.53	−2737.9	300–2000
k	low P∼10	1.17×10^{-6}	−2.02	−1205.6	300–2000
k	760	1.30×10^{-6}	−2.01	−805.2	300–2000

[a] $k(T) = AT^n\exp(-E_a/RT)$. Unit of the rate constants $k(T)$ is (cm^3 $molecule^{-1}$ s^{-1}) and k_0 is (cm^6 $molecule^{-2}$ s^{-1}).

Table 9. Arrhenius parameters[a] including high-pressure limit (k_∞) and low-pressure limit (k_0) for the $^2HSiSiH_2 + {}^1H_2 \rightarrow {}^2Si_2H_5$ and $^2HSiSiH_2 + {}^1H_2 \rightarrow {}^2SiH + {}^1SiH_4$ reactions.

	P (Torr)	A	*n*	E_a/R (K)	*T* range (K)
$^2HSiSiH_2 + {}^1H_2 \rightarrow {}^2Si_2H_5$					
k_∞	∞	2.22×10^{15}	−9.23	8436.0	300–2000
k_0	–	1.27×10^{8}	−13.09	6960.2	300–2000
k	0.3	9.72×10^{18}	−13.44	7061.2	300–2000
k	0.4	2.40×10^{19}	−13.51	7089.4	300–2000
k	0.5	5.27×10^{19}	−13.58	7116.0	300–2000
k	0.6	1.02×10^{20}	−13.63	7138.9	300–2000
k	1	9.86×10^{20}	−13.83	7234.8	300–2000
k	10	1.26×10^{28}	−15.35	8301.2	300–2000
k	760	1.79×10^{36}	−16.18	11205.7	300–2000
$^2HSiSiH_2 + {}^1H_2 \rightarrow {}^2SiH + {}^1SiH_4$					
k	10^6	2.17×10^{-5}	−3.66	6501.6	300–2000
k	low P∼10	2.22×10^{15}	−9.23	8436.0	300–2000
k	760	1.14×10^{17}	−9.70	9249.9	300–2000

[a] $k(T) = AT^n\exp(-E_a/RT)$. Unit of the rate constants $k(T)$ is (cm^3 $molecule^{-1}$ s^{-1}) and k_0 is (cm^6 $molecule^{-2}$ s^{-1}).

Table 10. Arrhenius parameters[a] including high-pressure limit (k_∞) and low-pressure limit (k_0) for the $^1Si_2H_4$ (C_{2h}) + $^2H \rightarrow {}^2Si_2H_5$ and $^1Si_2H_4$ (C_{2h}) + $^2H \rightarrow {}^2SiH + {}^1SiH_4$ reactions.

	P (Torr)	A	*n*	E_a/R (K)	*T* range (K)
$^1Si_2H_4$ (C_{2h}) + $^2H \rightarrow {}^2Si_2H_5$					
k_∞	∞	5.41×10^{14}	−8.31	2438.8	300–2000
k_0	–	2.26×10^{-7}	−7.88	1477.1	300–2000
k	0.3	7.27×10^{2}	−7.89	1423.8	300–2000
k	0.4	1.01×10^{3}	−7.89	1415.4	300–2000
k	0.5	1.27×10^{3}	−7.89	1405.1	300–2000
k	0.6	1.55×10^{3}	−7.89	1396.6	300–2000
k	1	2.67×10^{3}	−7.90	1362.2	300–2000
k	10	8.10×10^{4}	−8.01	1005.7	300–2000
k	760	3.54×10^{20}	−11.42	1944.2	300–2000
$^1Si_2H_4$ (C_{2h}) + $^2H \rightarrow {}^2SiH + {}^1SiH_4$					
k	10^6	8.25×10^{4}	−5.63	1981.6	300–2000
k	low P∼760	5.41×10^{14}	−8.31	2438.8	300–2000

[a] $k(T) = AT^n\exp(-E_a/RT)$. Unit of the rate constants $k(T)$ is (cm^3 $molecule^{-1}$ s^{-1}) and k_0 is (cm^6 $molecule^{-2}$ s^{-1}).

Acknowledgments

The authors deeply appreciate a partial support of this work by the Ministry of Economics under contract no. 98-EC-17-A-07-S2-0043. M.C.L. wants to thank the National Science Council of Taiwan for the support of this work and for the distinguished visiting professorship at the National Chiao Tung University in Hsinchu, Taiwan.

Keywords: Si_2H_5 · a-Si:H thin film · *ab initio* · chemical kinetics · plasma enhanced chemical vapor deposition

How to cite this article: S.-Y. Wu, Y.-M. Lee, J. S. Wu, M. C. Lin. *Int. J. Quantum Chem.* **2014**, *114*, 278–288. DOI: 10.1002/qua.24557

[1] J. K. Rath, *Sol. Energy Mater.Sol. Cells* **2003**, *76*, 431.
[2] A. Matsuda, *Jpn. J. Appl. Phys.* **2004**, *43*, 7909.

[3] S. Nishizaki, K. Ohdaira, H. Matsumura, *Thin Solid Films* **2009**, *517*, 3581.
[4] J. M. Jasinski, R. Becerra, R. Walsh, *Chem. Rev.* **1995**, *95*, 1203.
[5] S. Nakamura, K. Matsumoto, A. Susa, M. Koshi, *J. Non Cryst. Solids* **2006**, *352*, 919.
[6] A. A. Onischuk, V. N. Panfilov, *Russ. Chem. Rev.* **2001**, *70*, 321.
[7] U. V. Bhandarkar, M. T. Swihart, S. L. Girshick, U. R. Kortshagen, *J. Phys. D Appl. Phys.* **2000**, *33*, 2731.
[8] H. K. Motfat, K. F. Jensen, R. W. Carr, *J. Phys. Chem.* **1992**, *96*, 7695.
[9] K. Tonokura, T. Murasaki, M. Koshi, *J. Phys. Chem. B* **2002**, *106*, 555.
[10] S. Y. Wu, P. Raghunath, J. S. Wu, M. C. Lin, *J. Phys. Chem. A* **2010**, *114*, 633.
[11] B. Ruscic, J. Berkowitz, *J. Chem. Phys.* **1991**, *95*, 2416.
[12] D. Sillars, C. J. Bennett, Y. Osamura, R. I. Kaiser, *Chem. Phys.* **2004**, *305*, 141.
[13] A. D. Becke, *J. Chem. Phys.* **1993**, *98*, 5648.
[14] A. D. Becke, *Phys. Rev. A* **1998**, *38*, 3098.
[15] C. Lee, W. Yang, R. G. Parr, *Phys. Rev. B* **1988**, *37*, 785.
[16] (a) J. A. Pople, M. Head-Gordon, K. Raghavachari, *J. Chem. Phys.* **1987**, *87*, 5968; (b) R. Ditchfield, W. J. Hehre, J. A. Pople, *J. Chem. Phys.* **1971**, *54*, 724.
[17] C. Gonzalez, H. B. Schlegel, *J. Chem. Phys.* **1989**, *90*, 2154.
[18] C. Gonzalez, H. B. Schlegel, *J. Phys. Chem. A* **1990**, *94*, 5523.
[19] K. A. Peterson, D. E. Woon, T. H. Dunning, Jr., *J. Chem. Phys.* **1994**, *100*, 7410.
[20] D. E. Woon, Jr., T. H. Dunning, *J. Chem. Phys.* **1995**, *103*, 4572.
[21] M. J. Frisch, G. W. Trucks, H. B. Schlegel, G. E. Suseria, M. A. Robb, J. R. Cheeseman, J. J. A. Montgomery, T. K. Vreven, K. N. Kudin, J. C. Burant, J. M. Millam, S. S. Iyengar, J. Tomasi, V. Barone, B. Mennucci, M. Cossi, G. Scalmani, N. Rega, G. A. Petersson, H. Nakatsuji, M. Hada, M. Ehara, K. Toyota, R. Fukuda, J. Hasegawa, M. Ishida, T. Nakajima, Y. Honda, O. Kitao, H. Nakai, M. Klene, X. Li, J. E. Knox, H. P. Hratchian, J. B. Cross, C. Adamo, J. Jaramillo, R. Gomperts, R. E. Stratmann, O. Yazyev, A. J. Austin, R. Cammi, C. Pomelli, J. W. Ochterski, P. Y. Ayala, K. Morokuma, G. A. Voth, P. Salvador, J. J. Dannenberg, V. G. Zakrzewski, S. Dapprich, A. D. Daniels, M. C. Strain, O. Farkas, D. K. Malick, A. D. Rabuck, K. Raghavachari, J. B. Foresman, J. V. Ortiz, Q. Cui, A. G. Baboul, S. Clifford, J. Cioslowski, B. B. Stefanov, G. Liu, A. Liashenko, P. Piskorz, I. Komaromi, R. L. Martin, D. J. Fox, T. Keith, M. A. Al-Laham, C. Y. Peng, A. Nanayakkara, M. Challacombe, P. M. W. Gill, B. Johnson, W. Chen, M. W. Wong, C. Gonzalez, J. A. Pople, Gaussian 03, Revision C.02; Gaussian Inc.: Wallingford, CT, **2004**.
[22] B. C. Garrett, D. G. Truhlar, *J. Phys. Chem.* **1979**, *83*, 1052.
[23] C. -C. Hsu, A. M. Mebel, M. C. Lin, *J. Chem. Phys.* **1996**, *105*, 2346.
[24] A. Fernández-Ramos, J. A. Miller, S. J. Klippenstein, D. G. Truhlar, *Chem. Rev.* **2006**, *106*, 4518.
[25] M. W. J. Chase, NIST-JANAF thermochemical tables, 4th ed.; J. Phys. Chem. Ref. Data Monogr. 9, Parts I and II, NIST, Washington DC, USA. **1998**.
[26] T. Baer, W. L. Hase, Unimolecular Reaction Dynamics Theory and Experiments; Oxford University Press: New York, **1996**.
[27] C. -C. Hsu, M. C. Lin, A. M. Mebel, C. F. Melius, *J. Phys. Chem.* **1997**, *101*, 60.
[28] S. J. Klippenstein, A. F. Wagner, R. C. Dunbar, D. M. Wardlaw, S. H. Robertson, VariFlex, Version 1.0; Argonne National Laboratory: Argonne, IL, **1999**.
[29] J. Berkowitz, J. P. Greene, H. Cho, B. Ruscic, *J. Chem. Phys.* **1987**, *86*, 1235.
[30] L. A. Curtiss, K. Raghavachari, P. W. Deutsch, J. A. Pople, *J. Chem. Phys.* **1991**, *95*, 2433.
[31] A. F. Sax, J. Kalcher, *J. Phys. Chem.* **1991**, *95*, 1768.
[32] A. M. Doncaster, R. Walsch, *Int. J. Chem. Kinet.* **1981**, *13*, 503.
[33] N. S. Shuman, A. P. Spencer, T. Baer, *J. Phys. Chem. A* **2009**, *113*, 9458.
[34] A. Bodi, J. P. Kercher, C. Bond, P. Meteesatien, B. Sztray, T. Baer, *J. Phys. Chem. A* **2006**, *110*, 13425.
[35] R. L. Burden, J. D. Faires, Numerical Analysis, 8th ed; Thomson Brooks/Cole, Boston, USA, **2005**.
[36] M. E. Coltrin, R. J. Kee, J. A. Miller, *J. Electrochem. Soc.* **1986**, *133*, 1206.
[37] A. Barbato, C. Seghi, C. Cavallotti, *J. Chem. Phys.* **2009**, *130*, 074108.
[38] M. C. Lin, K. J. Laidler, *Can. J. Chem.* **1968**, *46*, 973.

Received: 14 June 2013
Revised: 1 August 2013
Accepted: 10 September 2013
Published online 7 October 2013